Science
AAAS

Water-promoted interfacial pathways in methane oxidation to methanol on a CeO_x-Cu_2O catalyst

Authors: Zongyuan Liu[1†], Erwei Huang[2†], Ivan Orozco[2], Wenjie Liao[2], Robert M. Palomino[1], Ning Rui,[1] Thomas Duchon[3], Slavomir Nemsak[4], David Grinter,[5] Mausumi Mahapatra[1], Ping Liu[1,2,*], José A. Rodriguez [1,2,*], Sanjaya D. Senanayake [1,*]

Affiliations:

[1]Chemistry Division, Brookhaven National Laboratory, Upton, NY 11973 USA.

[2]Chemistry Department, Stony Brook University, Stony Brook, NY 11794 USA.

[3]Peter-Grünberg-Institut 6, Forschungszentrum Jülich, 52425 Jülich, Germany.

[4]Advanced Light Source, Lawrence Berkeley National Laboratory, Berkeley, CA 94720, USA.

[5]Diamond Light Source Limited, Diamond House, Harwell Science and Innovation Campus, Didcot, Oxfordshire OX11 0DE, U.K.

*Correspondence to: pingliu3@bnl.gov (P.L.); rodrigez@bnl.gov (J.A.R.); ssenanay@bnl.gov (S.D.S)

†Dr. Z. Liu and E. Huang contributed equally to this work and should be regarded as co-first authors.

Abstract: Highly selective oxidation of methane to methanol has long been challenging in catalysis. Here, we reveal key steps for the promotion by water when tuning the selectivity of a well-defined $CeO_x/Cu_2O/Cu(111)$ catalyst from CO and CO_2 to methanol under a reaction environment with methane, oxygen and water. Ambient-pressure x-ray photoelectron spectroscopy showed that water added to CH_4 and O_2 led to surface CH_3O and accelerated methanol production. These results were consistent with density functional theory calculations and kinetic Monte Carlo simulations which showed that water preferentially dissociates over the active Ce ions at the CeO_2-$Cu_2O/Cu(111)$ interface. The adsorbed OH blocked O-O bond cleavage that would dehydrogenate CH_3O to CO and CO_2, , and it directly converted this species to methanol, whileO_2 now reoxidized the reduced surface. Water adsorption also displaced the produced methanol into the gas phase.

One Sentence Summary: New mechanistic insights on the role of water in the direct catalytic conversion of methane to methanol.

Main Text:. Methane (CH_4), the main component of natural gas, is difficult to upgrade to value added chemicals (aromatics, olefins, oxygenates) or even hydrogen (H_2) because of its strong C-H bonds (104 kcal/mol). In nature, enzymes use oxygen-containing molecules such as water (H_2O), oxygen (O_2), and carbon dioxide (CO_2) to convert CH_4 to methanol (CH_3OH) at ambient temperature directly, unlike commercial process that require the energy-intensive formation of syngas (H_2 and CO) (*1-4*). Applying such biomimetic strategies to heterogeneous catalysts is often limited by the need for high temperatures that lead to poor selectivity (*5-11*), but some oxide and metal/oxide surfaces can dissociate CH_4 at room temperature, which opens the possibility for a direct $CH_4 \rightarrow CH_3OH$ conversion (*12-13*). Indeed, a $Ni/CeO_2(111)$ catalyst can directly synthesize CH_3OH on exposure to a mixture of CH_4, O_2 and H_2O. The selectivity of the process is rather low

(<40%) (*14*). On the other hand, an inverse catalyst of the $CeO_2/Cu_2O/Cu(111)$ type displays a CH_4 to CH_3OH selectivity close to 70% (*16*).

Extensive studies have investigated the reaction mechanism, including the active sites, the nature of reaction intermediates, the operating pathway and the role of O_2 and H_2O in the $CH_4 \rightarrow CH_3OH$ conversion. Some studies have proposed O_2 as the oxidizing agent for conversion of CH_4 to CH_3O and CH_3OH through the generation of an active metal=O species on the catalyst surface at high temperature (450 to 500 K) (*10, 14, 17-19*). H_2O can help in the hydrogenation of CH_3O or block surface sites preventing its decomposition and facilitating the extraction of methanol (*10, 11, 14*). In the case of Cu-containing zeolites that mimic enzymes, CH_3OH generation is a sequential process that involves treatment or activation with O_2, reaction with CH_4, and finally extraction with water (*6, 7, 11, 20*). For the active $CeO_2/Cu_2O/Cu(111)$ catalyst, the origin of the high selectivity (~ 70%) toward CH_3OH remains elusive.

We combined ambient-pressure x-ray photoelectron spectroscopy (AP-XPS) with density functional theory (DFT) calculations and kinetic Monte Carlo (KMC) simulation and obtained direct evidence for the essential role of H_2O in the selective production of CH_3OH upon exposure of CH_4, O_2 and H_2O over the $CeO_2/Cu_2O/Cu(111)$ catalyst. The spectroscopic measurement and theoretical modeling agreed that H_2O acts not only as an extractor of CH_3OH as previously reported (*10, 11, 14*), but more importantly as a blocker and active chemical reagent. The addition of H_2O blocks the metal=O mediated mechanism proposed previously (*10, 14, 17-19*) and prevents the complete dissociation of CH_4 to form CO or CO_2, and opens a new *OH-mediated pathway, which enables the activation of CH_4 for direct CH_3OH formation at the CeO_2-$Cu_2O/Cu(111)$ interface. Direct $CH_4 \rightarrow CH_3OH$ conversion by *OH opens new opportunities to more active and selective catalysts for CH_4 utilization.

Both Cu-containing enzymes (*3, 4*) and zeolites (*6, 10, 11*) convert CH_4 into CH_3OH. The oxidation state of the copper in these systems is usually assumed to be +2 before reaction with CH_4 and +1 after CH_4 activation (*6*). In AP-XPS experiments, we found a very low reactivity of plain $Cu_2O/Cu(111)$ systems toward CH_4 at room temperature. But this system and ceria are very active for water dissociation *(15, 21)*. The deposition of cerium on $Cu_2O/Cu(111)$ under an atmosphere of O_2 (5×10^{-7} torr) leads to formation of two types of islands, as shown by images of scanning tunneling microscopy (STM) (*22*). Large islands of ceria (30 to 50 nm in size and triangular shape) were embedded in the substrate step edges and had a morphology different from that seen for the two most stable surfaces of bulk ceria: $CeO_2(111)$ and $CeO_2(110)$ (*22*). These islands had a high of ~ 0.3 nm, which was consistent with a single layer of cerium sandwiched in between two layers of oxygen. In addition to the large ceria islands, a small concentration of small ceria islands formed that were 0.5 to 5 nm in size (*16,22*).

As shown in Fig. 1A, exposing a $CeO_x/Cu_2O/Cu(111)$ surface (θ_{CeO2}= 0.5) to 20 mTorr of CH_4 at 300 K resulted in two peaks at ~287.0 eV and 285.3 eV in the C 1s region, which we attributed to the CH_4 gas phase and surface -CH_x species, respectively (*14*). The formation of -CH_x resulted from the dissociative adsorption of CH_4 at room temperature at a coverage of ~ 0.15 monolayer (ML). The hydrocarbon fragment had a relatively strong surface bond as it is still adsorbed on surface at 450 K At this temperature, an additional feature grew in 289.4 eV that corresponded to CO_x groups formed by the reaction between surface O sites and C atoms produced by the full decomposition of CH_4 (*14*). Thus, in contrast to plain $Cu_2O/Cu(111)$, the $CeO_2/Cu_2O/Cu(111)$ surface exhibited substantial reactivity toward CH_4.

The C 1s XPS acquired while exposing CuO_2/Cu(111) and several CeO_2/CuO_2/Cu(111) surfaces to 20 mTorr of CH_4 at 300 K are compared in Fig. 1B. After normalization by the intensity of the peak for gaseous CH_4, the most active CeO_2/Cu_2O/Cu(111) system was that with a ceria coverage near 0.5 ML (Fig. 1C). A 1.5 ML ceria system was not very active, probably because the ceria-copper oxide interface was substantially reduced and ceria deactivated when two-dimensional (2D) islands grew into three-dimensional (3D) ones (*22*). When these AP-XPS results are compared with data of catalytic activity for the conversion of CH_4 on CeO_2/Cu_2O/Cu(111) (*16*), one finds excellent agreement between the ability of the surface to activate CH_4 at room temperature and its activity for the conversion of the hydrocarbon to CH_3OH or a CO/CO_2 mixture. A CeO_2/Cu_2O/Cu(111) system with 0.5 ML of ceria exhibited the best performance for CH_4 activation and conversion.

Over Cu-containing zeolites, CH_3OH is produced by the sequential steps of activation in O_2, reaction with CH_4 and extraction with H_2O (*6, 7, 11, 20*). After sequentially adding 10 mTorr of O_2 into the chamber at 450 K (CH_4/O_2 reaction feed), no changes were seen in the C 1s XPS region for Cu_2O/Cu(111) and CeO_2/Cu_2O/Cu(111) surfaces. In particular, no CH_3O peak around 286.5 eV was detected. This result is consistent with the lack of CH_3OH formation over these surfaces where only CO and CO_2 are detected as reaction products in the absence of H_2O (*16*). Although O_2 dissociates readily on CeO_x/Cu_2O/Cu(111) (*23*), a metal-O or metal=O group is not an efficient agent for the formation of CH_3OH on these surfaces. A CH_3O intermediate could be formed, but it probably would decompose very rapidly on some active sites of the surface (see DFT calculations below) producing mainly CO/CO_2 and not give a signal in AP-XPS (*16*).

The addition of H_2O to the CH_4/O_2 reaction mixture induced drastic changes in the chemical process. On CeO_2/Cu_2O/Cu(111), water dissociated to form OH on the surface at 300 and 450 K as seen in AP-XPS (Fig. S1). Signals for OH species bound to Cu_2O (~531.1 eV) *(15)* and ceria (~532.1 eV) *(21)* were observed in the O 1s region (Fig. S1). Fig. 2A shows C 1s XPS spectra collected while exposing a CeO_2/Cu_2O/Cu(111) surface (θ_{CeO2}= 0.5) to a set of $CH_4/O_2/H_2O$ reactants at temperatures between 300 and 450 K. In the presence of water, one can see a clear change in the C 1s features with signals not seen in the case of a dry experiment, where only moderate amounts of CH_x and CO_x are detected (for an example, see Fig. 1A). The spectra in Fig. 2A were curve fitted (Fig. S2) well with peaks for $CO_{x,ads}$, $CH_{4,gas}$, CH_3O_{ads}, $CH_{x,ads}$ and C_{ads} *(24)*. In test experiments for the adsorption of CH_3OH and its derivatives, the features around 286.2 eV corresponded to adsorbed CH_3O, in good agreement with previous XPS studies (*25, 26*). As mentioned above, this species was not seen after exposing the surfaces to a simple CH_4/O_2 reaction mixture. Furthermore, in Fig. 2A, the adsorbed CH_3O was seen at temperatures of 400 and 450 K, which were the onset for a catalytic $CH_4 \rightarrow CH_3OH$ transformation over CeO_2/Cu_2O/Cu(111) surfaces exposed to a mixture of $CH_4/O_2/H_2O$ (*16*).

Figure 2B compares C 1s spectra collected after exposing a CeO_2/Cu_2O/Cu(111) surface (θ_{CeO2}= 0.5) to CH_4, $CH_4 + O_2$, $CH_4 + H_2O$, and $CH_4 + H_2O + O_2$ at 450 K, a threshold for CH_3OH production (*16*). The amounts of CH_x and CH_3O present on the catalyst surface under pure CH_4 and a CH_4/O_2 mixture were negligible. Thus, a reaction feed of CH_4/O_2 produced mainly (~ 95%) CO and CO_2 as products (*16*). CH_3O and CH_x appeared when H_2O is added to the reaction feed, but the amount of CH_3O was larger when a mixture of $CH_4/O_2/H_2O$ is used (Fig. S3), and the CH_3O signal in AP-XPS was correlated with the CH_3OH selectivity measured in catalytic tests (Fig. 2C). At high temperatures, CH_4 alone could induce a partial reduction of the ceria overlayer (Fig. S4), but under a mixture of $CH_4/O_2/H_2O$, the ceria remained fully oxidized (Fig. S5). And

there was not reduction of the Cu_2O film in between ceria and Cu(111). Although the $CeO_2/Cu_2O/Cu(111)$ system has special properties for the dissociation of CH_4 (Fig. 1), some of its sites were probably too reactive to allow any CH_3O formed to avoid decomposition. The OH groups coming from water dissociation (*22*) were necessary to block these sites and, as we will see below, they also could participate in an additional reaction path for the activation and conversion of CH_4 .

Our AP-XPS measurements were fully consistent with the theoretical calculations using DFT and the KMC simulation under the experimental conditions (pressure ratio: $CH_4 : O_2 = 2:1$ or $CH_4 : O_2 : H_2O = 2: 1 : 8$; T= 450K, see SI for details). In the DFT calculations, the $CeO_2/Cu_2O/Cu(111)$ catalyst was modeled by depositing a Ce_3O_6 cluster on the 44 structure of $Cu_2O/Cu(111)$ (Fig. S6A, see SI for detail and (*16*). [note referee comment about the cluster used] According to the DFT results, the $CeO_2/Cu_2O/Cu(111)$ system should produce mainly CO_2 from a CH_4/O_2 mixture following a reaction path that is highly exothermic (Fig. S7 and S8). Initially, upon exposure to CH_4 and O_2, an active Ce site (Ce-2 in Fig.S6B) at the CeO_2-$Cu_2O/Cu(111)$ interface stabilized O_2 (binding energy or E_{ads} = -14.53 kcal/mol) [given the expts are in kcal/mol, it would be better to report the energies the same way here] and enabled the facile O-O bond cleavage with the synergy of Cu from the Cu_2O film (reaction energy or ΔE = -24.44 kcal/mol; activation barrier or E_a = 5.54 kcal/mol, Fig. 3A). However, in this case, none of the terminal metal=O oxo ligands, which were previously proposed as the active sites for CH_4 to CH_3OH conversion for the zeolite-based systems (*10, 17-19*), survived. Instead, the doubly bridging oxo ligand formed (*O) over the interfacial Cu-Ce bridge sites (Fig. 3A and S7).

The CH_4 also preferred the same Ce site; yet the KMC simulations show that it could not compete with O_2 because of weakened binding (E_{ads} = -2.54 kcal/mol) and the elevated barrier for dissociation (E_a = 11.76 kcal/mol) (*16*). Thus, all active Ce sites at the $CeO_2/Cu_2O/Cu(111)$ were occupied by *O from O_2 dissociation. The formed doubly bridging oxo Ce-O-Cu species were active to adsorb (E_{ads} = -1.15 kcal/mol) and activate CH_4 through the preferential C-O bond association. Either methoxy (*CH_3O) species (ΔE = -37.82 kcal/mol, E_a = 18.45 kcal/mol, Fig. S7 and S8) formed, or *CH_3OH formed directly at the interface (E_a = 16.37 kcal/mol). The KMC simulations, however, demonstrated that the produced *CH_3OH was not stable and preferentially dissociated to *CH_3O with no barrier (ΔE = -14.53 kcal/mol).

The sequential dehydrogenation of *CH_3O to *CH_2O, *CHO and eventually production of CO_2 was highly favorable in terms of both thermodynamics and kinetics according to the DFT calculations (Fig. S7), and hence none of the intermediates was likely to be stable. Indeed, under steady states the $CeO_2/Cu_2O/Cu(111)$ surface remained clean on exposure to CH_4 and O_2, as demonstrated by the KMC snapshot (Fig. S9). No *CH_3O or other adsorbed surface species could be observed, which agreed well with the AP-XPS measurements in Fig. 2B and 2C for the experiment with a CH_4/O_2 reaction feed. Regarding the products in the catalytic tests (*16*), the KMC results were consistent with the experimental results (Fig. 2C), showing that $CeO_2/Cu_2O/Cu(111)$ was highly selective to CO_2/CO on exposure to CH_4 and O_2 rather than CH_3OH (Fig. 4A). Finally, during the dehydrogenation process, oxygen vacancies (O_v, Fig. S7 and Fig. S8) were generated on the supported CeO_2 cluster, that could be quickly filled in presence of O_2 as reported previously (*16*).

The addition of H_2O in the mixture of CH_4 and O_2 changed the reaction network on the catalyst surface. First, H_2O blocked the adsorptions and dissociation of O_2 at the active interfacial Ce site (Fig. 3A), as seen under exposure of CH_4 and O_2. According to the DFT calculations, H_2O

also preferred (E_{ads}= -15.91 kcal/mol), as did O_2, to adopt a tilted conformation [please check my edit, but the original was not clear, and picking out one structure in fig S9 and S10 is not obvious] because of the formation of hydrogen bond with nearby bridging oxygen (Fig. 3A, S10 and S11). The tilted adsorption was followed by a spontaneous O-H bond cleavage (Fig. 3A), which was much more facile than the O-O (E_a = 5.54 kcal/mol) and C-H bond breakage (E_a = 11.76 kcal/mol) (*16*). Also, the pressure of H_2O was eight times higher than that of O_2 under reaction conditions considered in both experiment and KMC simulations. Thus [the next sentence on adsorption doesn't follow in an obvious way—did the KMC sims also use this pressure ratio?], the KMC simulations showed that the adsorption rate of O_2 decreased by a factor of ~30 by the addition of H_2O. In this case, 90% of active Ce sites were occupied by hydroxyl (*OH) from H_2O dissociation and only 10% formed the Ce-O-Cu oxo species, as was the case without H_2O. Thus, the adsorbed *OH groups blocked reactive Ce sites from interaction with O_2 and in the presence of H_2O, new reaction paths are enabled to facilitate CH_3OH production (Fig. 3A, S10 and S11).

The *OH species generated by H_2O dissociation at the interfacial Ce sites opened a new highly effective pathway for a real catalytic transformation (Fig. 3B and S10). Along the new path, the direct conversion from CH_4 to $*CH_3OH$ is substantially populated by the active *OH at the Ce site (Fig. 3B and S10) through the concerted C-O bond association and C-H dissociation (ΔE = -18.68 kcal/mol, E_a = 22.37 kcal/mol). This step represented the rate-limiting step along the path and the negative shift in barrier by 0.1 eV can effectively increase the CH_4 conversion by 93.79% and CH_3OH selectivity by 3.78%. This reaction is followed by the barrierless dissociation to $*CH_3O$, as was for the CH_4 oxidation by O_2. The difference is that the presence of H_2O predominantly blocked the $*CH_3O$ decomposition and thus the formation of CO_2. Instead, H_2O also enabled the extraction of CH_3OH from $*CH_3O$, or the removal of $*CH_3O$ as gas phase CH_3OH, in addition to blocking O_2 adsorption and activating CH_4.

This process started with the formation of $*CH_3O\cdots HOH$ through hydrogen bonding (Fig. 3C and S12). This structural motif drove the proton hopping from H_2O to $*CH_3O$ (ΔE = 4.85 kcal/mol, E_a = 6.69 kcal/mol, Fig. 3C and S12) and produces gas phase CH_3OH and the active *OH to replace the binding site for $*CH_3O$ at interfacial Ce site, which is active for direct $CH_4 \rightarrow CH_3OH$ conversion (Fig. 3B and S10). The dissociated *H from CH_4 resulted in the hydroxylation of CeO_2 (Fig. S10 and S11), which could easily be removed with the assistance of $*H_2O$ at the Ce site, leading to the formation of oxygen vacancy (O_v) and thus the reduced CeO_x (ΔE = -8.30 kcal/mol, E_a = 2.31 kcal/mol, Fig. S10). At this point, O_2 could preferentially fill the O_v and re-oxidize CeO_x to CeO_2 (Fig. S10), which is the dominant role of O_2 during this process due to the preferential O_2 dissociation (E_a = 3.00 kcal/mol) over H_2O dissociation (E_a = 15.45 kcal/mol) at the O_v site.

According to the KMC simulations, under steady states of CH_4 oxidation by O_2 and H_2O, the $CeO_2/Cu_2O/Cu(111)$ surface was not clean anymore. Instead, two stable surface species, *OH and $*CH_3O$ (Fig. 4B), which agreed very well with measurements of AP-XPS (Fig. 2B). Both surface species bound to the supported CeO_2 at the interface (Fig. S13). The formation of *OH was associated with H_2O and CH_4 dissociation, and $*CH_3O$ is formed because of the interplay between the barrierless O-H bond cleavage of $*CH_3OH$ and the activated extraction of CH_3OH from $*CH_3O$ by H_2O (Fig. 3C, S7 and S10).

The amount of *OH present on the catalyst surface was larger than the amount of $*CH_3O$ (Fig 4B), a condition which was essential to prevent the full oxidation of the formed $*CH_3O$

species. The stabilized *CH_3O and the enabled *CH_3O extraction by adding of H_2O to the mixture of CH_4 and O_2 tuned the selectivity of $CeO_2/Cu_2O/Cu(111)$ from CO_2 to CH_3OH as the major product according to the KMC simulations (Fig. 4A), which was also observed by the AP-XPS measurements and catalytic tests [Fig. 2C and (*16*)]. The addition of H_2O also facilitated the CH_3OH production through oxidation of CH_4 by O_2 by hindering the *CH_3O dehydrogenation and promoting the extraction of CH_3OH according to the KMC simulation results (Fig. 3C and S13). About one half of the dissociated *O at the active Ce sites led to the CH_3OH production, and the rest remained as oxidizing agent to produce CO_2. Yet, because of lower adsorption rate of O_2 than H_2O at the active Ce sites, 95% of produced CH_3OH is by reaction with H_2O, and the dominant roles that O_2 plays is to fill the O_v sites via facile dissociation. [as meant? O2 just reoxidizes Ce]

The AP-XPS data were consistent with the results of combined DFT and KMC simulations, showing that on the active CeO_2-Cu_2O interfaces, CH_4 was preferentially oxidized by O_2 into CO and CO_2 (Fig. S14A). When H_2O is added to a CH_4/O_2 mixture, the selectivity was tuned toward CH_3OH (Fig. S14B). The $CeO_2/Cu_2O/Cu(111)$ inverse catalyst exhibited a reactivity different from that reported for zeolite-based materials during the selective oxidation of CH_4. On the zeolite-based catalysts, O_2 is considered as the oxidizing agent and H_2O is just extracting [there has to be a better word—displacing?] the formed *CH_3OH.

However, on $CeO_2/Cu_2O/Cu(111)$, H_2O played three key roles. As on a zeolite-based material, H_2O acted as a site blocker. It preferentially occupied the active Ce sites at the CeO_2-Cu_2O interface, which hindered the O_2 activation and thus the conversion of CH_4 to CO or CO_2 (Fig.3A). More importantly, it was an active center, where the facial dissociation at the interfacial Ce sites produced the active *OH, being able to open a new pathway and promote the direct CH_4 to CH_3OH conversion (Fig.3B). In this case, H_2O participated in the reaction directly as the actual O-provider and enables the direct CH_4 to CH_3OH conversion. In this system, O_2 only helped to re-oxidize CeO_x, which was partially reduced during the reaction. Finally, H_2O functioned as an extractor as proposed previously, preventing the dehydrogenation of *CH_3O and thus CO_2 formation, while facilitating the hydrogenation and thus CH_3OH formation (Fig.3C). The identification of the key roles played by H_2O while tuning the selectivity during CH_4 conversion points to phenomena that must be taken into consideration when dealing with new routes for designing efficient catalyst for the selective $CH_4 \rightarrow CH_3OH$ oxidation.

References and Notes:

1. A. C. Rosenzweig, C. A. Frederick, S. J. Lippard, P. Nordlund, Crystal structure of a bacterial non-haem iron hydroxylase that catalyses the biological oxidation of methane. *Nature* **366**, 537-543 (1993).
2. S. Sirajuddin, A. C. Rosenzweig, Enzymatic oxidation of methane. *Biochemistry* **54**, 2283-2294 (2015).
3. M. O. Ross, F. MacMillan, J. Wang, A. Nisthal, T. J. Lawton, B. D. Olafson, S. L. Mayo, A. C. Rosenzweig, B. M. Hoffman, Particulate methane monooxygenase contains only mononuclear copper centers. *Science* **364**, 566-570 (2019).
4. R. Balasubramanian S. M. Smith, S. Rawat, L. A. Yatsunyk, T. L. Stemmler, A. C. Rosenzweig, Oxidation of methane by a biological dicopper centre. *Nature* **465**, 115-119 (2010).

5. M. Ravi, M. Ranocchiari, A. van Bokhoven Jeroen, The direct catalytic oxidation of methane to methanol - A critical assessment. *Angew. Chem. Int. Ed.* **56**, 16464-16483 (2017).

6. V. L. Sushkevich, D. Palagin, M. Ranocchiari, J. A. van Bokhoven, Selective anaerobic oxidation of methane enables direct synthesis of methanol. *Science* **356**, 523-527 (2017).

7. S. Grundner, M. A. Markovits, G. Li, M. Tromp, E. A. Pidko, E. J. Hensen, A. Jentys, M. Sanchez-Sanchez, J. A. Lercher, Single-site trinuclear copper oxygen clusters in mordenite for selective conversion of methane to methanol. *Nat. Commun.* **6**, 7546 (2015).

8. J. Shan, M. Li, L. F. Allard, S. Lee, M. Flytzani-Stephanopoulos, Mild oxidation of methane to methanol or acetic acid on supported isolated rhodium catalysts. *Nature* **551**, 605-608 (2017).

9. C. Hammond, M. M. Forde, M. H. Ab Rahim, A. Thetford, Q. He, R. L. Jenkins, N. Dimitratos, J. A. Lopez-Sanchez, N. F. Dummer, D. M. Murphy, A. F. Carley, S. H. Taylor, D. J. Willock, E. E. Stangland, J. Kang, H. Hagen, C. J. Kiely, G. J. Hutchings, Direct catalytic conversion of methane to methanol in an aqueous medium by using copper-promoted Fe-ZSM-5. *Angew. Chem. Int. Ed.* **51**, 5129-5133 (2012).

10. M. H. Groothaert, P. J. Smeets, B. F. Sels, P. A. Jacobs, R. A. Schoonheydt, Selective oxidation of methane by the bis (μ-oxo) dicopper core stabilized on ZSM-5 and mordenite zeolites. *J. Am. Chem. Soc.* **127**, 1394-1395 (2005).

11. P. Tomkins, A. Mansouri, S. E. Bozbag, F. Krumeich, M. B. Park, E. M. C. Alayon, M. Ranocchiari, J. A. van Bokhoven, Isothermal cyclic conversion of methane into methanol over copper-exchanged zeolite at low temperature. *Angew. Chem. Int. Ed.* **55**, 5467-5471 (2016).

12. Z. Liang, T. Li, M. Kim, A. Asthagiri, J. F. Weaver, Low-temperature activation of methane on the IrO2 (110) surface. *Science* **356**, 299-303 (2017).

13. Z. Liu, P. Lustemberg, R. A. Gutierrez, J. J. Carey, R. M. Palomino, M. Vorokhta, D. C. Grinter, D. C.; P. J. Ramirez, V. Matolin, M. Nolan, M. V. Ganduglia-Pirovano, S. D. Senanayake, J. A. Rodriguez, In-situ investigation of methane dry reforming on metal/ceria(111) surfaces: Metal–support interactions and C−H bond activation at low temperature. *Angew. Chem. Int. Ed.* **56**, 13041-13046 (2017).

14. P. G. Lustemberg, R. M. Palomino, R. A. Gutierrez, D. C. Grinter, M. Vorokhta, Z. Liu, P. J. Ramirez, V. Matolin, M. V. Ganduglia-Pirovano, S. D. Senanayake, J. A. Rodriguez, Direct conversion of methane to methanol on Ni-ceria surfaces: Metal–support interactions and water-enabled catalytic conversion by site blocking. *J. Am. Chem. Soc.* **140**, 7681-7687 (2018).

15. X. Deng, T. Herranz, C. Weis, H. Bluhm, M. Salmeron, Adsorption of water on Cu_2O and Al_2O_3 thin films. *J. Phys. Chem. C* **112**, 9668-9672 (2008).

16. Z. Zuo, P. J. Ramírez, S. D. Senanayake, P. Liu, J. A. Rodriguez, Low-temperature conversion of methane to methanol on CeO_x/Cu_2O catalysts: water controlled activation of the C–H bond. *J. Am. Chem. Soc.* **138**, 13810-13813 (2016).

17. P. J. Smeets, R. G. Hadt, J. S. Woertink, P. Vanelderen, R. A. Schoonheydt, B. F. Sels, E. I. Solomon, Oxygen precursor to the reactive intermediate in methanol synthesis by Cu-ZSM-5. *J. Am. Chem. Soc.* **132**, 14736-14738 (2010).

18. J. S. Woertink, P. J. Smeets, M. H. Groothaert, M. A. Vance, B. F. Sels, R. A. Schoonheydt, E. I. Solomon, A $[Cu_2O]^{2+}$ core in Cu-ZSM-5, the active site in the oxidation of methane to methanol. *Proc. Natl. Acad. Sci. U.S.A.* **106**, 18908-18913 (2009).

19. G. Li, P. Vassilev, M. Sanchez-Sanchez, J. A. Lercher, E. J. M. Hensen, E. A. Pidko, Stability and reactivity of copper oxo-clusters in ZSM-5 zeolite for selective methane oxidation to methanol. *J. Catal.* **338**, 305-312 (2016).

20. P. Tomkins, M. Ranocchiari, J. A. van Bokhoven, Direct conversion of methane to methanol under mild conditions over Cu-zeolites and beyond. *Acc. Chem. Res.* **50**, 418-425 (2017).

21. J. Carrasco, D. López-Durán, Z. Liu, T. Duchoň, J. Evans, S. D. Senanayake, E. J. Crumlin, V. Matolín, J. A. Rodríguez, M. V. Ganduglia-Pirovano, In situ and theoretical studies for the dissociation of water on an active Ni/CeO_2 catalyst: Importance of strong metal–support interactions for the cleavage of O–H bonds. *Angew. Chem. Int. Ed.* **54**, 3917-3921 (2015)

22. J. A. Rodriguez, J. Graciani, J. Evans, J. B. Park, F. Yang, D. Stacchiola, S. D. Senanayake, S. Ma, M. Pérez, P. Liu, J. F. Sanz, J. Hrbek, Water-gas shift reaction on a highly active inverse CeO_x/Cu(111) Catalyst: Unique role of ceria nanoparticles. *Angew. Chem. Int. Ed.* **48**, 8047-8050 (2009).

23. F. Yang, J. Graciani, J. Evans, P. Liu, J. Hrbek, J. F. Sanz, J. A. Rodriguez, CO oxidation on inverse CeO_x/Cu(111) catalysts: High catalytic activity and ceria-promoted dissociation of O_2. *J. Am. Chem. Soc.* **133**, 3444-3451 (2011).

24. Y. Lykhach, T. Staudt, M. P. A. Lorenz, R. Streber, A. Bayer, H.-P. Steinrück, J. Libuda, Microscopic insights into methane activation and related processes on Pt/ceria model catalysts. *ChemPhysChem* **11**, 1496-1504 (2010).

25. A. Siokou, R. M. Nix, Interaction of methanol with well-defined ceria surfaces: Reflection/absorption infrared spectroscopy, X-ray photoelectron spectroscopy, and temperature-programmed desorption study. *J. Phys. Chem. B* **103**, 6984-6997 (1999).

26. D. R. Mullins, Variations in the surface chemistry of methanol with CeO_2(100) at low and elevated pressures. *Surf. Interface Anal.* **50**, 913-920 (2018).

27. G. Kresse, J. Furthmüller, Efficiency of ab-initio total energy calculations for metals and semiconductors using a plane-wave basis set. *Comput. Mater. Sci.* **6**, 15-50 (1996).

28. C. T. Campbell, L. Árnadóttir, J. R. V. Sellers, Kinetic prefactors of reactions on solid surfaces. *Z. Phys. Chem.* **227**, 1435-1454 (2013).

29. S. Kattel, P. J. Ramírez, J. G. Chen, J. A. Rodriguez, P. Liu, Active sites for CO_2 hydrogenation to methanol on Cu/ZnO catalysts. *Science* **355**, 1296-1299 (2017).

30. NIST computational chemistry comparison and benchmark database. http://cccbdb.nist.gov/.

Refs 26 to 44 appear in this list and NOT in the SM, thx

Acknowledgments:

Funding: The research carried out at Brookhaven National Laboratory (BNL), was supported by the U.S. Department of Energy, Office of Science and Office of Basic Energy Sciences under contract No. DE-SC0012704. X-ray spectroscopy measurements were performed at beamline 9.3.2 at the Advanced Light Source of LBNL, which is a DOE Office of Science User Facility under

contract no. DE-AC02-05CH11231. The DFT calculations were performed using computational resources at the Center for Functional Nanomaterials, a U.S. DOE Office of Science Facility, and the Scientific Data and Computing Center, a component of the Computational Science Initiative at BNL under Contract No. DE-SC0012704, at the National Energy Research Scientific Computing Center (NERSC), a DOE Office of Science User Facility, supported by the Office of Science of the DOE under contract DE-AC02-05CH11231 and at Stony Brook University, which was founded by National Science Foundation grant (#1531492). SDS is partially supported by a U.S. DOE Early Career Award. **Author contributions:** P.L., J.A.R. and S.D.S. came with the general idea and supervised the execution of the project and written of the article. Z.L and E.H. worked in the main writing of the manuscript. Z.L., R.M.P., T.D., S.N. and D.C.G. performed synchrotron photoemission experiments at the ALS. I.O., N.R. and M.M. did studies with XPS and morphology characterization. E.H and W.L. performed the theoretical calculations. **Competing interests:** The authors declare no competing financial interests. **Data and materials availability:** All data is available in the main text or the supplementary materials.

Supplementary Materials:

Materials and Methods

Figures S1-S13

Tables S1-S2

References (*27-30*)

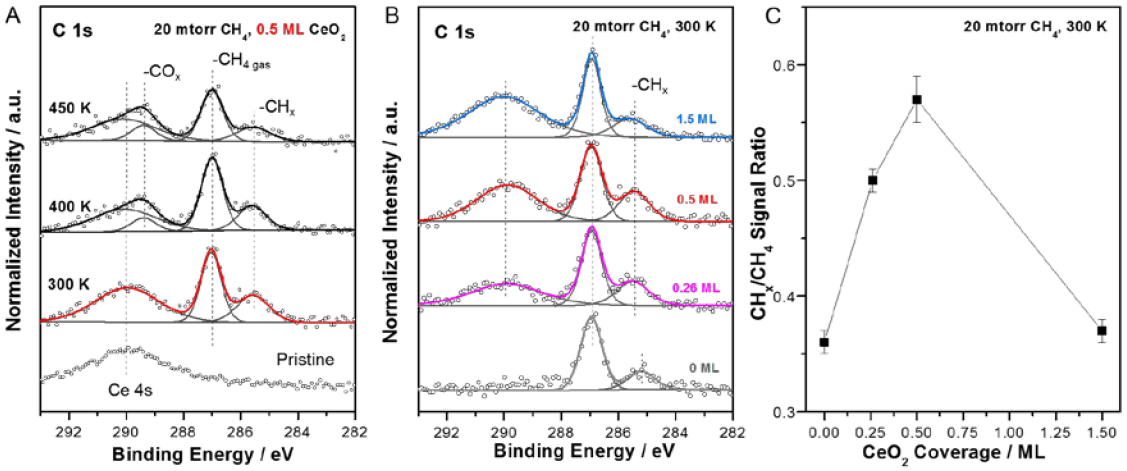

Fig. 1. Methane interaction with $CeO_2/Cu_2O/Cu(111)$. C 1s region of the AP-XPS spectra for introducing 20 mTorr of CH_4 to (A) 0.5 ML CeO_2 covered $Cu_2O/Cu(111)$ surface at different temperatures, (B) different coverages of ceria on $Cu_2O/Cu(111)$ surface at 300 K. (C) Comparison

of the surface -CH_x amount derived from the integration of the corresponding C 1s normalized peak in (B).

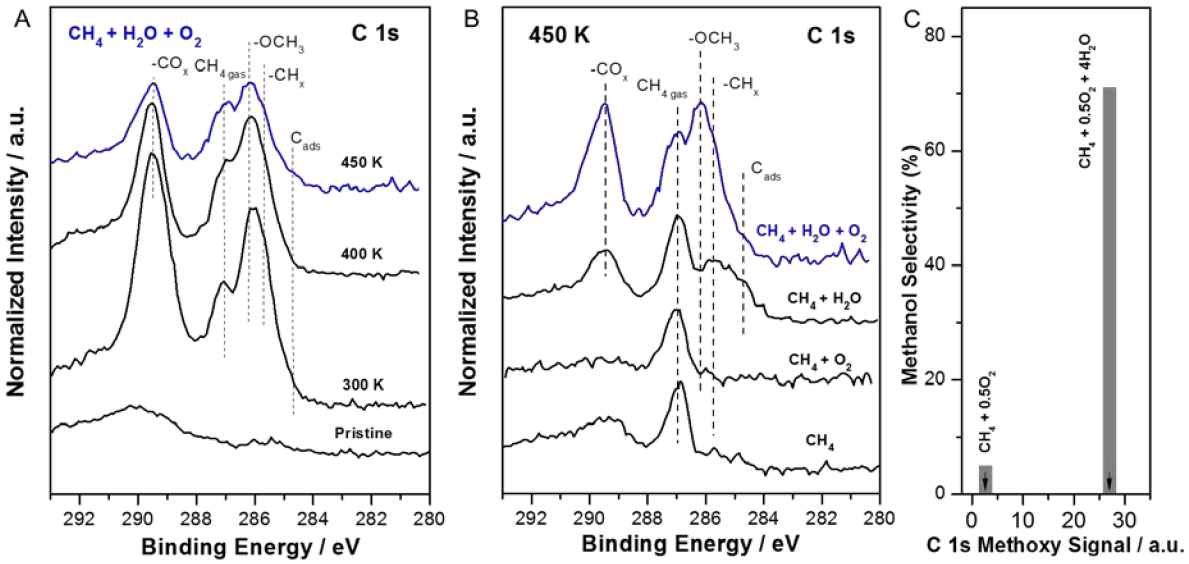

Fig. 2. Water effects on methoxy formation on $CeO_2/Cu_2O/Cu(111)$. C 1s region of the AP-XPS spectra for (A) the $CeO_2/Cu_2O/Cu(111)$ surface (θ_{CeO2}~ 0.5 ML) when exposed to a 20 mTorr CH_4 + 80 mTorr H_2O + 10 mTorr O_2 of gas mixture at different temperatures, (B) comparison of exposing $CeO_2/Cu_2O/Cu(111)$ surfaces (θ_{CeO2}~ 0.5 ML) to different gas reactants at 450 K. (C) CH_3OH

selectivity versus the amount of -CH_3O generated with and without addition of water. The results for the catalytic tests were taken from. (*16*).

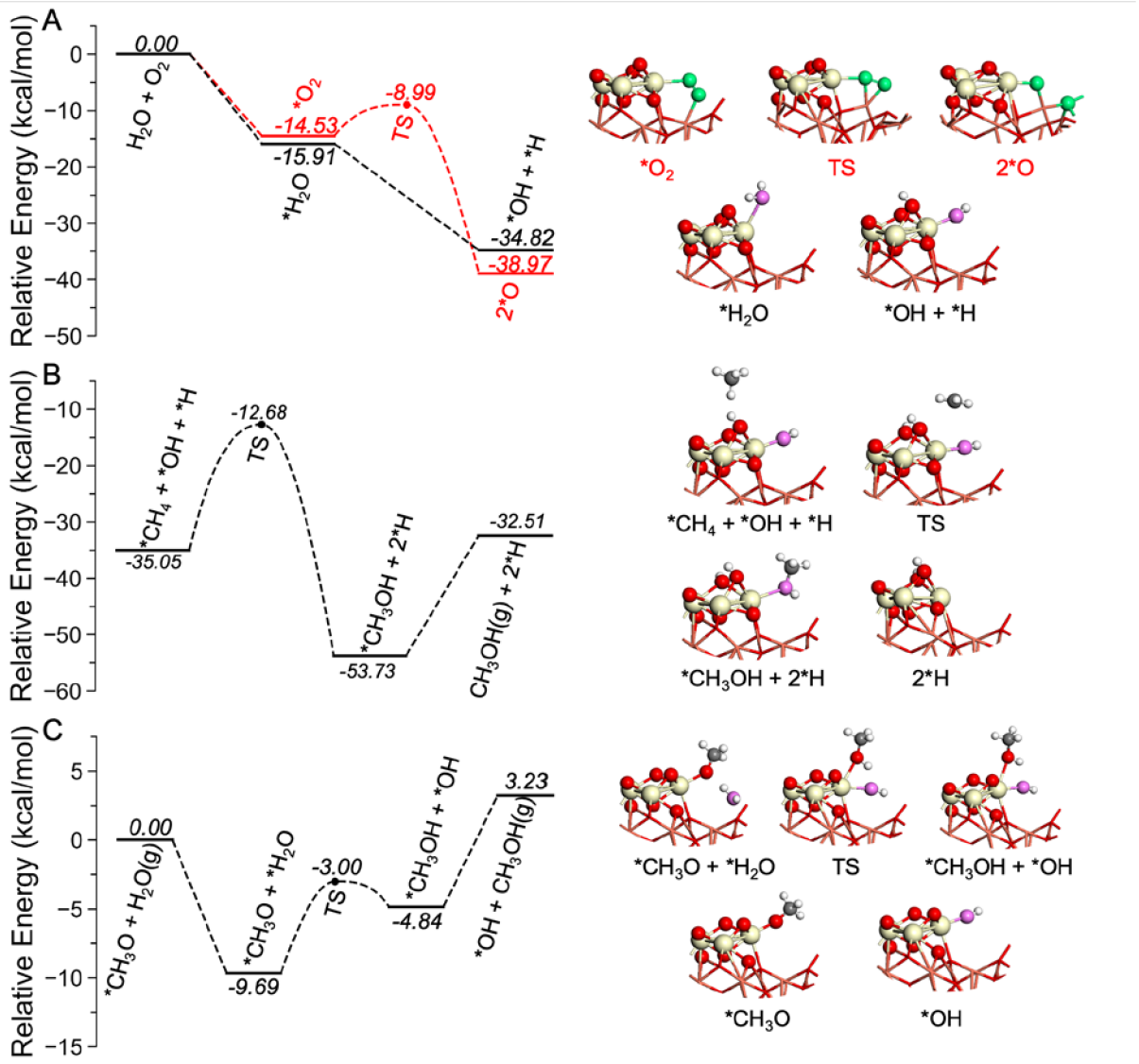

As the referee noted, this is not very accessible – some heading in the figure, telling what is happening (absorption, what bond breaks or forms, etc) would help. It's not clear that all of the intermediates here are needed, as it's difficult to focus on key steps. The three roles of water should be clearly indicated as well. Also give the energy in kcal/mole on an axis on the right sides

Fig. 3. DFT-calculated potential energy diagrams for the three important steps involved in CH_4 oxidation by O_2 and H_2O on $CeO_2/Cu_2O/Cu(111)$. (**A**) O_2 and H_2O dissociation, showing the preferential H_2O dissociative adsorption and thus the blocked active Ce sites from O_2 by H_2O; (B) CH_4 oxidation by *OH, demonstrating the enabled one-step CH_3OH synthesis from CH_4 by dissociated fragments from H_2O; (C) Hydrogenation of $*CH_3O$ by H_2O, indicating the facilitated CH_3OH formation or extraction by H_2O. The structures of intermediates and transition states (TS)

were also included. Yellow: Ce; brown: Cu; red: O in CeO_2/Cu_2O/Cu(111) (A) and *CH_xO (B); green: O in O_2; purple: O in H_2O; gray: C; white: H.

5

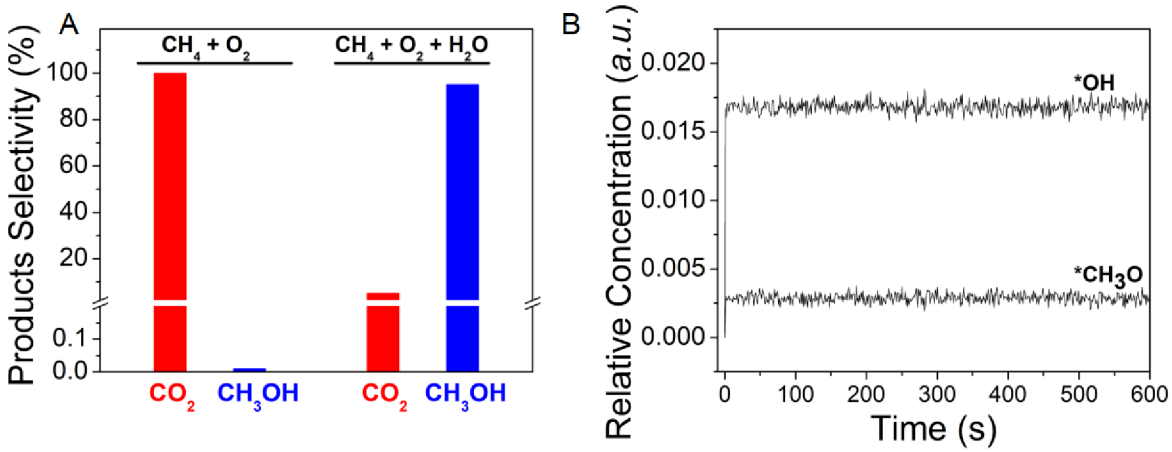

Fig. 4. KMC-simulated product selectivity and reaction intermediates. (**A**) Selectivity of CH_4 oxidation over $CeO_2/Cu_2O/Cu(111)$ on exposure to CH_4 and O_2 with pressure ratio of 2:1 or CH_4, O_2 and H_2O with pressure ratio of 2:1:8 at 450K. (**B**) Coverage of adsorbed surface species on $CeO_2/Cu_2O/Cu(111)$ under the mixture of CH_4, O_2 and H_2O.